KSME

Springer

Journal of Mechanical Science and Technology 34 (9) 2020

Original Article
DOI 10.1007/s12206-020-0838-4

Keywords:
· Design fire curves
· Fire dynamics simulator
· Large eddy simulation
· Mixing controlled fast chemistry
· Mixture fraction
· Tunnel fire

Correspondence to:
Chang Bo Oh
cboh@pknu.ac.kr

Citation:
Myilsamy, D., Oh, C. B., Lee, C. Y. (2020). Numerical investigation of prediction performance of design fire curves for a tunnel fire. Journal of Mechanical Science and Technology 34 (9) (2020) 3875~3887. http://doi.org/10.1007/s12206-020-0838-4

Received March 16th, 2020
Revised May 27th, 2020
Accepted June 18th, 2020

† Recommended by Editor
Yong Tae Kang

Numerical investigation of prediction performance of design fire curves for a tunnel fire

Dinesh Myilsamy[1], Chang Bo Oh[1] and Chi Young Lee[2]

[1]Department of Safety Engineering, Pukyong National University, Busan 48513, Korea, [2]Department of Fire Protection Engineering, Pukyong National University, Busan 48513, Korea

Abstract The prediction performance of design fire curves is numerically investigated for tunnel fire using the fire dynamics simulator (FDS). A large eddy simulation (LES) was adopted in the simulation of a previous 750 kW tunnel fire experiment. Based on the experimental heat release rate, t^2-fire growth, quadratic and exponential design fire curves (DFCs) are mathematically constructed and adopted in the FDS simulation. The predictions of each DFCs are compared against the experimentally measured smoke temperature, smoke travel time, and carbon monoxide (CO) concentration. In addition, the prediction performance of the mixture fraction (MF) and mixing controlled fast chemistry (MCFC) combustion models, is compared. The simulation results of the MF and MCFC models are similar except for the CO concentration features. For the performance of the DFCs, t^2-fire growth curve with the MF combustion model is the most effective combination, which demonstrated the most reasonable agreement with the experimental data.

1. Introduction

Tunnel transportation is a fast and efficient transportation system, especially in urban and mountainous areas. In addition, tunnel transportation reduces noise pollution and traffic congestion in cities. However, when a tunnel fire accident occurs, it causes catastrophic damage to human life and transportation facilities. Many sever tunnel fire accidents in road tunnels have occurred worldwide, such as those in St. Gotthard (1997), Mont Blanc (1999), Kaprun (2000), Tauern (2002), Trojane (2011), and Gudvanga (2013) tunnels [1]. To understand the potential risks involved in tunnel fire accidents and to enhance public safety, various tunnel fire studies have been performed [2-8]. However, tunnel fire experiments are complex, difficult to reproduce, and expensive. In addition, it is not feasible to perform experiments with many different fire scenarios. Hence, numerical simulations with appropriate fire scenarios have been performed to overcome the challenges in tunnel fire experiments.

Numerical simulations provide the flexibility of solving complex problems efficiently. They can provide three-dimensional visualization of fire spread, smoke flow movement, and toxic gas production rate with sufficient accuracy. Many simulations for tunnel fires have been performed [4, 5, 8-11], which studies primarily focused on toxic gas production and smoke flow physics involved in tunnel fire experiments. Furthermore, the experimental fire condition was used as the initial fire input. However, simulations employing only the experimental fire condition are limited in representing various tunnel fire scenarios because the scenarios for fire risk assessment should include various fire growth, maximum and decay phases. For the consolidation and convenient simulation of tunnel fires, a design fire curve (DFC) was developed as an initial condition of fire scenarios [12].

A DFC can represent either the worst-case fire scenario or a conceivable fire scenario and is used to estimate a reasonable upper bound of the consequence [13]. A design fire can be represented as a heat release rate (HRR), fire load density, and production rate of combustion products. Kim et al. [14] demonstrated the importance of the HRR for estimating fire growth and

Table 1. Mathematical description of design fire curves.

t^2-fire growth curve	Growth phase	$\dot{Q} = \alpha_g t^2$, $(t = t - t_O)$
	Maximum phase (modified)	$\dot{Q}_{max,av} = \frac{\sum_{t_{lo}}^{td} \dot{Q}}{t_d - t_{lo}}$
	Decay phase	$\dot{Q} = \alpha_d t^2$, $(t = t_{end} - t)$
Quadratic curve	Growth phase	$\dot{Q}(t) = \alpha_{g,q} t^2$, $(0 \le t_{max})$
	Maximum phase	$\dot{Q}(t) = \alpha_{g,q} t_{max}^2 = \dot{Q}_{max}$, $(t_{max} < t < t_D)$
	Decay phase	$\dot{Q}(t) = \dot{Q}_{max} e^{-\alpha_{D,q}(t-t_D)}$, $(t \ge t_D)$
Exponential curve	Growth, maximum & decay phase	$\dot{Q}(t) = \dot{Q}_{max}\, n\, r \left(1 - e^{-kt}\right)^{n-1} e^{-kt}$, $(t \ge 0)$ $k = \frac{\dot{Q}_{max}}{E_{tot}} r$, $r = \left(1 - \frac{1}{n}\right)^{1-n}$

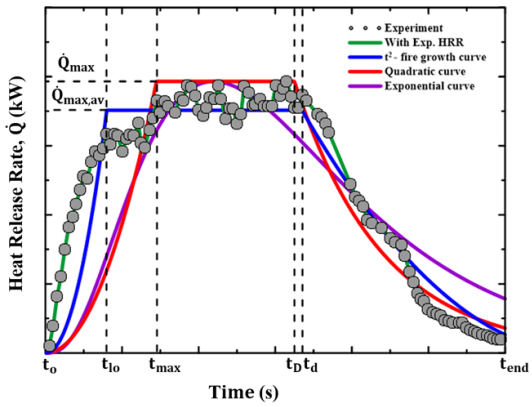

Fig. 1. Comparison of temporal HRR variations obtained by experiment and approximated DFCs.

temperature in structural fires. Babrauskas and Peacock [15] considered the HRR as one of the most crucial variables in fire hazard analysis. Therefore, the DFC is typically expressed as a simple mathematical form by combining the maximum HRR with different fire growths and decay rates.

Ingason [16] developed a mathematical form to calculate the HRR and time required to attain the maximum HRR and fire duration in fuel-controlled fires in tunnels. Kim and Lilley [17] suggested a simple form of a t^2-fire growth curve to express fire behavior and flashover. Ingason [12] suggested different DFCs and demonstrated that the length of the maximum HRR constant period depended on the total heat content of the fire load. For risk assessments, numerical simulations with DFCs provide many advantages for investigating fire behaviors in tunnels with different fire scenarios. However, the prediction performance of the suggested DFCs through the simulation of tunnel fires has not been validated by comparing it with experimental results.

Hence, the main objective of this study is to investigate the prediction performance of previously suggested t^2-fire growth [14, 17, 18], quadratic, and exponential DFCs [12] for tunnel fires by adopting DFCs in numerical simulations as an input condition. The simulations were performed using the fire dynamics simulator (FDS) developed by the National Institute of Standards and Technology (NIST) with a large eddy simulation (LES) approach. Mixture fraction (MF) and mixing controlled-fast chemistry (MCFC) combustion models were used in the simulation to determine the effects of the models. The simulation results with each DFC were validated by comparing them with the temperature, smoke travel time, and CO concentration obtained in a previous tunnel fire experiment [7].

2. DFCs

In this study, t^2-fire growth [14, 17, 18], quadratic, and exponential DFCs [1, 12] were based on previous experimental HRR data for tunnel fire [7] using the mathematical expressions shown in Table 1. These DFCs were used in the simulations of tunnel fire as an initial fire condition. The t^2-fire growth curve is the most widely used in building and structural fire safety analyses. The DFCs used for building fire safety analysis are primarily focused on the fire growth rate to address unique fire development scenarios that may occur in building fires [1]. However, the quadratic and exponential design fire curves were originally designed for tunnel fires.

Fig. 1 shows the temporal HRR variations obtained experimentally [7] and the approximated DFCs. The numerical values for the mathematical expressions of the DFCs are shown in Table 2. The HRR growth rate expressions of the quadratic and t^2-fire growth curves are similar, but the value and duration of the maximum HRR and decay phase modelling differ. The growth, maximum, and decay phases of an exponential design fire can be represented as a single mathematical expression. Exponential DFCs are primarily applicable for fuel-controlled fires and fires with a negligible constant maximum HRR phase [12]. It is noteworthy that the level-off time (t_{lo}) and the decay phase starting time (t_d) for the t^2-fire-growth curve were obtained from mathematical approximations. The studies of Kim

Table 2. Numerical values of design fire curves parameters.

	$\dot{Q}_{max,av}$ $(\dot{Q}_{max})$	t_O	t_{lo} (t_{max})	t_d (t_D)	t_{end}	α_g $(\alpha_{g,q})$	α_d $(\alpha_{D,q})$	n	r	q
t^2-fire growth curve	702.4	0.0	80.0	335.0	700.0	0.1125	0.0052	-	-	-
Quadratic curve	786.0	-	145.0	325.0	-	0.0373	0.0086	-	-	-
Exponential curve	786.0	-	-	-	-	-	-	4.0022	2.3705	0.0063

et al. [14, 17, 18] used 1 MW as a reference HRR value to model the fire growth rate (α_g). In addition, it is complex to determine the t_{lo} and t_d instants for a continuously fluctuating HRR curve. However, in this study, the maximum HRR is 785.4 kW and the HRR curve fluctuates continuously with time. Therefore, the t^2-fire growth formulation used by Kim et al. [14, 17, 18] requires modifications to model the constant maximum phase of a continuously fluctuating HRR curve. Thus, the $\dot{Q}_{max,av}$ approximated by averaging the HRR over the period between the instants of 80 % of the peak HRR values. The t_{lo} and t_d instants were determined from the first and last instants of 80 % of the peak HRR value. The α_g and α_d was calculated from the approximated t_{lo} and t_d instants and the obtained $\dot{Q}_{max,av}$ value found to be approximately 90 % of the maximum peak HRR value. Also, the preliminary design fire studies of Baek et al. [19] showed the maximum peak HRR value is not so important in DFC modelling when the $\dot{Q}_{max,av}$ is over 70 % of its maximum peak. Detailed descriptions of t^2-fire growth, quadratic, and exponential DFCs are available in Refs. [14, 17, 18] and Refs. [1, 12], respectively. The calculation procedures for the quadratic and exponential DFCs were the same as those in the original studies [1, 12].

3. Numerical methods

3.1 Governing equations

The FDS developed by NIST was used to investigate the prediction performance of DFCs for tunnel fires. The FDS solves low-Mach-number approximated governing equations for low speed, thermally driven flows. Filtered LES governing equations of mass, momentum, species and enthalpy were as follows:

Mass:

$$\frac{\partial \bar{\rho}}{\partial t}+\frac{\partial \bar{\rho}\tilde{u}_i}{\partial x_i}=0\,. \tag{1}$$

Momentum:

$$\frac{\partial \bar{\rho}\tilde{u}_i}{\partial t}+\frac{\partial}{\partial x_j}\left(\bar{\rho}\tilde{u}_i\tilde{u}_j\right)=-\frac{\partial \bar{p}}{\partial x_i}-\frac{\partial \bar{\tau}_{ij}}{\partial x_j}-\frac{\partial \tau_{ij}^{sgs}}{\partial x_j}+\bar{\rho}g_i\,. \tag{2}$$

Species:

$$\frac{\partial\left(\bar{\rho}\tilde{Y}_\alpha\right)}{\partial t}+\frac{\partial\left(\bar{\rho}\tilde{u}_i\tilde{Y}_\alpha\right)}{\partial x_i} =-\frac{\partial}{\partial x_i}\left(\overline{\rho u_i Y_\alpha}-\bar{\rho}\tilde{u}_i\tilde{Y}_\alpha\right)+\frac{\partial}{\partial x_i}\left(\bar{\rho}D_\alpha\frac{\partial \tilde{Y}_\alpha}{\partial x_i}\right)+\overline{\dot{m}_\alpha^{'''}}\,. \tag{3}$$

Enthalpy:

$$\frac{\partial \bar{\rho}\tilde{h}_s}{\partial t}+\frac{\partial\left(\bar{\rho}\tilde{u}_i\tilde{h}_s\right)}{\partial x_i}=\frac{D\bar{p}}{Dt}+\dot{q}^{'''}-\frac{\partial \dot{q}_r^{''}}{\partial x_i}+\frac{\partial}{\partial x_i}\left(k\frac{\partial \tilde{T}}{\partial x_i}\right)+\sum_\alpha\frac{\partial}{\partial x_i}\left(\bar{\rho}D_\alpha\tilde{h}_\alpha\frac{\partial \tilde{Y}_\alpha}{\partial x_i}\right). \tag{4}$$

Equation of state:

$$\rho=\frac{\bar{p}\bar{W}}{RT}\,. \tag{5}$$

The FDS does not explicitly solve the energy conservation equation; instead velocity divergence is factored out from the Eq. (4).

$$\nabla\cdot \mathrm{u}=\frac{1}{\rho h_s}\left[\frac{D}{Dt}\left(\bar{p}-\rho h_s\right)+\dot{q}^{'''}+\dot{q}_r^{'''}-\nabla\cdot\dot{q}^{''}\right]. \tag{6}$$

The stress due to viscous forces is obtained from the total deviatoric stress. The total deviatoric stress $\left(\tau_{ij}^{dev}\right)$ is expressed as

$$\tau_{ij}^{dev}\equiv\bar{\tau}_{ij}+\tau_{ij}^{sgs}-\frac{1}{3}\tau_{kk}^{sgs}\delta_{ij}=-2\left(\mu+\mu_t\right)\times\left(\frac{1}{2}\left(\widetilde{\frac{\partial u_i}{\partial x_j}+\frac{\partial u_j}{\partial x_i}}\right)-\frac{1}{3}\left(\nabla\cdot\tilde{u}\right)\delta_{ij}\right). \tag{7}$$

The constant smagorinsky was used as a subgrid scale model for this study. The thermal conductivity and material diffusivity are related to the turbulent Schmidt, and Prandtl number, respectively. In the constant smagorinsky model of the FDS, the values of Sc_t and Pr_t were set to 0.5.

$$k_{LES}=\frac{\mu_{LES}c_p}{Pr_t} \tag{8}$$

$$\rho D_{LES}=\frac{\mu_{LES}}{Sc_t}\,. \tag{9}$$

A detailed description of the turbulence approach and subgrid scale model is available in Refs. [20-23].

3.2 Combustion model

In this study, the MF model of FDS version 5.5 and the

MCFC model of FDS version 6.3.2 were adopted to investigate the effects of the combustion model on the results of tunnel fire simulations.

3.2.1 MF model

FDS version 5.5 adopts an MF model that considers the following two-step reactions to enhance the CO prediction performance. In the MF model, species equations are not solved, but equations for the mixture fraction are solved as follows:

$$C_x H_y O_z N_a M_b + \nu'_{O_2} O_2 \rightarrow \nu_{H_2O} H_2O + \left(\nu'_{CO} + \nu_{CO}\right) CO + \nu_s S + \nu_{N_2} N_2 + \nu_M M \quad (10)$$

$$\nu'_{CO}\left[CO + \frac{1}{2} O_2 \rightarrow CO_2\right]. \quad (11)$$

Eq. (10) cosniders two stoichiometric coefficient ν'_{CO} and ν_{CO} for CO. ν'_{CO} is the stoichiometric coefficient for a well-ventilated fire that is later converted into CO_2, and ν_{CO} is the fixed CO production specified as the CO yield in the FDS by the user. The first reaction is based on a fast (instantaneous) reaction of fuel and oxygen to form CO and other products. The volumetric fuel consumption rate is computed as follows:

$$\dot{m}''_F = \frac{min\left(\rho Y_F, s\rho Y_{O_2}\right)}{\tau} \quad (12)$$

$$s = \frac{W_F}{\nu_{O_2} W_{O_2}} \quad (13)$$

$$\tau = \frac{C\left(\delta x \times \delta y \times \delta z\right)^{\frac{2}{3}}}{D_{LES}}. \quad (14)$$

The default emperical constant value (C = 0.1) was used in the simulation. The second-step reaction considers the finite rate reaction [19] to convert the CO to CO_2

$$k(T) = 2.53 \times 10^{12} e^{-199.547/RT}. \quad (15)$$

The two-step reactions requires three independent variables to track the amount of fuel, amount of fuel converted to CO, and amount of CO reacted to form CO_2. A linear combination approach was considered to derive the transport equations for fuel, CO and CO_2:

$$\frac{DY_F}{Dt} = \nabla \cdot D\rho \nabla Y_F + \dot{m}'''_{F,1} \quad (16)$$

$$\frac{DY_{CO}}{Dt} = \nabla \cdot D\rho \nabla Y_{CO} + \dot{m}'''_{CO,1} + \dot{m}'''_{CO,2} \quad (17)$$

$$\frac{DY_{CO_2}}{Dt} = \nabla \cdot D\rho \nabla Y_{CO_2} + \dot{m}'''_{CO_2,2}. \quad (18)$$

From Eqs. (16)-(18), transport equations for three submixture fraction varibales can be derived and expressed as the Eqs. (19)-(21), respectively. In the equations, the three submixture fractions are not conserved scalar.

$$\frac{DZ_1}{Dt} = \nabla \cdot D\rho \nabla Z_1 + \dot{m}'''_{F,1} \quad (19)$$

$$\frac{DZ_2}{Dt} = \nabla \cdot D\rho \nabla Z_2 - \dot{m}'''_{F,1} + \frac{W_F \dot{m}'''_{CO,2}}{\nu_{CO} W_{CO}} \quad (20)$$

$$\frac{DZ_3}{Dt} = \nabla \cdot D\rho \nabla Z_3 - \frac{W_F \dot{m}'''_{CO,2}}{\nu_{CO} W_{CO}} \quad (21)$$

where

$$Z_1 = Y_F;\ Z_2 = \frac{W_F}{\nu_{CO} W_{CO}} Y_{CO};\ Z_3 = \frac{W_F}{\nu_{CO_2} W_{CO_2}} Y_{CO_2}. \quad (22)$$

The final mixture fraction, is a conserved scalar, Z, can be calculated by the summation of all the three submixture fraction variables.

$$Z_1 + Z_2 + Z_3 = Y_F + \frac{W_F}{\nu_{CO} W_{CO}} Y_{CO} + \frac{W_F}{\nu_{CO_2 W_{CO_2}}} Y_{CO_2} = Z. \quad (23)$$

A diluent can be considered in the fuel or oxidizer stream in the MF concept. The diluent is assumed to be nitrogen, its mass fraction in the fuel stream is $Y^I_{N_2} = 1 - Y^I_F$ and the ambient mass fraction of oxygen and nitrogen is estimated from $Y^\infty_{N_2} = 1 - Y^\infty_{O_2}$. Accounting for fuel dilution, the three submixture fractions can be expressed as follows:

$$Z_1 = \frac{Y_F}{Y^I_F} \quad (24)$$

$$Z_2 = \frac{W_F}{W_{CO}\nu_{CO}} \frac{Y_{CO}}{Y^I_F} \quad (25)$$

$$Z_3 = \frac{W_F}{W_{CO_2}\nu_{CO_2}} \frac{Y_{CO}}{Y^I_F}. \quad (26)$$

The Mass fractions of each species were computed as follows:

$$Y_F = Z_1 Y^I_F \quad (27)$$

$$Y_{O_2} = (1 - Z) Y^\infty_{O_2} - \frac{W_{O_2} Y^I_F}{W_F}\left(\nu'_{O_2} Z_2 + \nu_{O_2} Z_3\right) \quad (28)$$

$$Y_{CO} = \frac{\left(\nu_{CO} + \nu'_{CO}\right) W_{CO_2}}{W_F} Y^I_F Z_2 \quad (29)$$

$$Y_{CO_2} = \frac{\nu_{CO_2} W_{CO_2}}{W_F} Y^I_F Z_3 \quad (30)$$

$$Y_{H_2O} = \frac{\nu_{H_2O} W_{H_2O}}{W_F} Y^I_F (Z_2 + Z_3) \quad (31)$$

$$Y_{N_2} = (1-Z)Y_{N_2}^{\infty} + Y_{N_2}^{I} Z_1 + \frac{\nu_{N_2} W_{N_2}}{W_F} Y_F^{I} (Z_2 + Z_3) \quad (32)$$

$$Y_s = \frac{\nu_s W_s}{W_F} Y_F^{I} (Z_2 + Z_3) . \quad (33)$$

The stoichiometric coefficients were calculated as follows:

$$\nu_{O_2} = \nu_{CO_2} + \frac{\nu_{CO} + \nu_{H_2O} - z}{2} \quad (34)$$

$$\nu_{O_2}^{'} = \frac{\nu_{CO}^{'} + \nu_{H_2O}}{2} \quad (35)$$

$$\nu_{CO} = \frac{W_F}{W_{CO}} y_{CO} \quad (36)$$

$$\nu_{CO}^{'} = x - \nu_{CO} - (1 - X_H)\nu_s \quad (37)$$

$$\nu_{CO_2} = x - \nu_{CO} - (1 - X_H)\nu_s \quad (38)$$

$$\nu_{H_2O} = \frac{y}{2} - X_H \nu_s \quad (39)$$

$$\nu_{N_2} = \frac{a}{2} \quad (40)$$

$$\nu_s = \frac{W_F}{W_s} y_s . \quad (41)$$

The heat release rate per unit volume for the first step was computed as follows:

$$\dot{q}''' = \dot{m}_F''' \Delta H_F . \quad (42)$$

After the first-step reaction if $\dot{q}''' \neq 0$, in a gird cell, then the heat release rate of the second-step is computed using Eq. (43):

$$\dot{q}_{CO}''' = min\left[\frac{max(\rho Z_2, s\rho Y_{O_2})}{\delta t} \Delta H_{CO}, \dot{q}_{max}''' - \dot{q}''' \right] . \quad (43)$$

After the first step reaction if $\dot{q}''' = 0$, in a grid cell, then the FDS assumes that the cell was outside of the combustion region, and a finite-rate reaction computation was performed to convert CO to CO_2. The heat release rate was computed using Eq. (44):

$$\dot{q}_{CO}''' = \rho \Delta H_{CO} \frac{dY_{CO}}{\delta t} . \quad (44)$$

A detailed description of the mixture fraction model is available in Refs. [20, 21, 24, 25].

3.2.2 MCFC model

A single-step MCFC combustion approach was implemented using FDS version 6.3.2. A typical hydrocarbon reaction to predict the CO concentration and soot for a single-step MCFC is as follows:

$$\nu_0 \left(\nu_{O_{2,0}} O_2 + \nu_{N_{2,0}} N_2 + \nu_{H_2O,0} H_2O + \nu_{CO_{2,0}} CO_2 \right) + \nu_1 \left(C_m H_n O_a N_b \right)$$
$$\rightarrow \nu_2 \left(\nu_{CO_2,2} CO_2 + \nu_{H_2O,2} H_2O + \nu_{N_2,2} N_2 + \nu_{CO,2} CO + \nu_{S,2} Soot \right) \quad (45)$$

where the CO yield and soot yield are user-specified values. The model for the species source term $\dot{m}_\alpha'''$ in the species transport equation is expressed as

$$\overline{\dot{m}_\alpha'''} = \rho \frac{d\tilde{Y}_\alpha}{dt} . \quad (46)$$

The mean chemical source term for the fuel is expressed as

$$\overline{\dot{m}_F'''} = -\bar{\rho} \frac{min\left(\tilde{Y}_F, \frac{\tilde{Y}_{O_2}}{s} \right)}{\tau_{mix}} . \quad (47)$$

The heat release rate per unit volume in the governing equation is obtained from the summation of species mass production rates and the respective heat of formation.

$$\dot{q}''' \equiv -\sum_\alpha \dot{m}_\alpha''' \Delta h_{f,\alpha}^0 . \quad (48)$$

A detailed description of the mixing controlled fast chemistry apporach is available in Refs. [22, 23].

3.3 Solution procedure

The FDS employs an explicit time-marching scheme as a solution procedure to solve fire-induced flows and is suitable for addressing a wide range of practical fire scenarios [26]. The governing equations were spatially discretized using a second-order accurate finite difference scheme. In the temporal discretization, the variables were advanced in time using a second-order accurate explicit predictor–corrector scheme. To treat the radiative source term, $\dot{q}_r''$ in the governing equation, a gray gas radiation model was adopted. A detailed description of the solution procedure and the numerical method for the radiation model are available in Refs. [20-23].

3.4 Computational setup

Numerical simulations were performed for a previous tunnel fire experiment involving a tunnel measuring 88 m × 8 m × 2.7 m [7]. Fig. 2(a) shows the tunnel geometry and burner location in the simulation. All numerical geometries of the tunnel and fire conditions were the same as those in the experiment. One end of the tunnel was fully closed, and its opposite end was half closed. The material of the tunnel ceiling was set to be gypsum, which filled the space of the ceiling thickness between 2.65 and 2.70 m; the sidewalls and floor were concrete. The material properties for the gypsum and concrete were referred

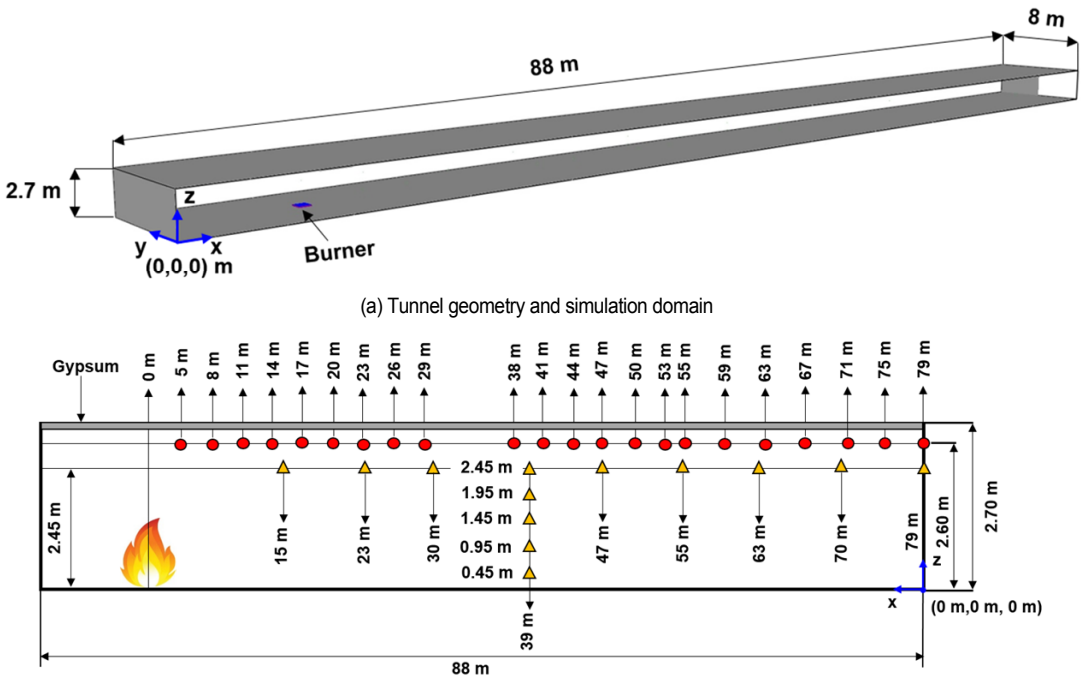

(a) Tunnel geometry and simulation domain

(b) Thermocouple and CO sensor locations

Fig. 2. Schematic representation of the tunnel geometry and the location of thermocouple and CO sensors in the simulation and experiment.

from the FDS user guide. The FDS code was based on the Cartesian coordinate system, and only rectangular geometries were allowed to be defined numerically. Hence, a rectangular burner was installed instead of the circular burner used in the experiment. However, the burner area of 0.6082 m^2 and its location were set to be the same as those in the experiment. Because an exact molecular formula is unavailable for the diesel fuel used in the experiment, an average chemical formula of $C_{12}H_{23}$ was used for the reaction, the soot yield value was set to 0.1 according to the studies of Hu et al. [7], and the CO yield was calculated based on the correlation developed by Köylü and Faeth [27]. The numerical thermocouple used and the CO sensor locations were specified according to the experimental conditions [7]. Fig. 2(b) shows the locations of the thermocouple and CO sensors. The longitudinal temperature and CO concentrations inside the tunnel were measured numerically at 2.60 m from the floor level from 7 to 79 m away from the fire source. In addition, vertical CO concentrations were measured 39 m away from the fire source at vertical heights of 0.95, 1.45, 1.95, and 2.45 m from the floor level, as shown in Fig. 2(b). In the figure, the red circle represents the thermocouple locations and the yellow triangle represents the CO sensor locations. A grid dependency test was performed with the grid sizes of 5 cm, 10 cm, and 15 cm and 20 cm. The computations were performed for the experimental fire scenario with the experimental HRR and MF combustion model. The time-averaged gas-phase temperature predicted by the different grid sizes were almost similar. The time-averaged CO predictions of 5 cm and 10 cm grids showed similar predictions to each other, whereas the 15 cm and 20 cm grids showed lower CO predictions than the 5 cm and 10 cm grids. Considering the computational time, 10 cm grid was adopted in the present simulations. The simulation domain was discretized into 1900800 grids with a uniform cell size of 10 cm. The simulations were performed using the message passing interface parallel technique on a 45-core PC-cluster machine with an Intel Core i7-4470K 3.50 GHz. The computational time for each simulation was approximately 530 to 551 CPU hours (~12 h of physical time). Simulations using the MF model were faster than those using the MCFC model by approximately 12.7 % based on CPU hours.

4. Results and discussion

4.1 Fire development behavior

Fig. 3 shows the temporal HRR variation obtained by experiment and simulations with three DFCs. The results show the effects of the combustion, MF, and MCFC models on the prediction of the HRR in tunnel fires. For comparison, the simulation results for the HRR with the experimental HRR as an input fire condition are plotted. The simulation results for the HRR are almost identical to the HRR input curves of each DFC, as shown in Fig. 1, except for some perturbations. The effects of the MF and MCFC models of the FDS on the prediction performance of the HRR were negligible. The HRR trend simulated with the experimental HRR input agreed well with the experimental results. The simulated fire growth rates with DFCs were slower than those in the experiment. Nevertheless, the t^2-fire growth curve demonstrated a better prediction performance for the fire growth trend compared with the quadratic

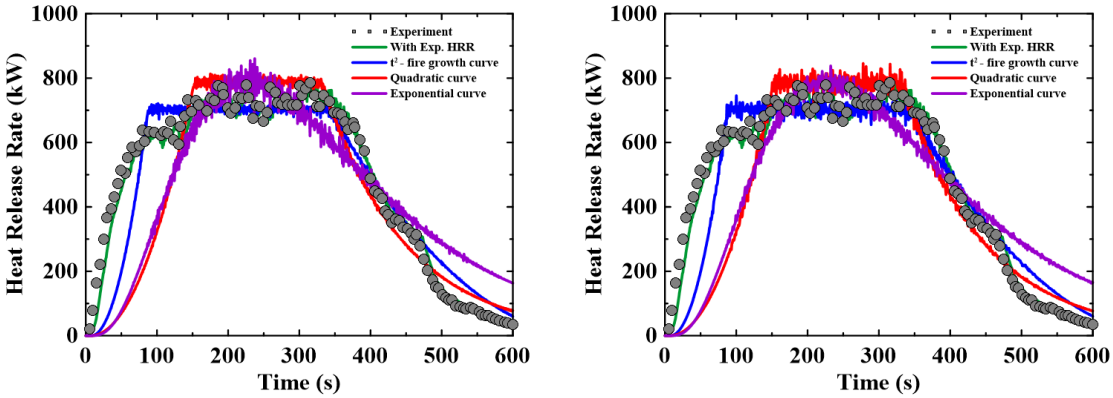

(a) MF (b) MCFC

Fig. 3. Temporal HRR variation obtained by experiment and simulations with the experimental HRR and three DFC.

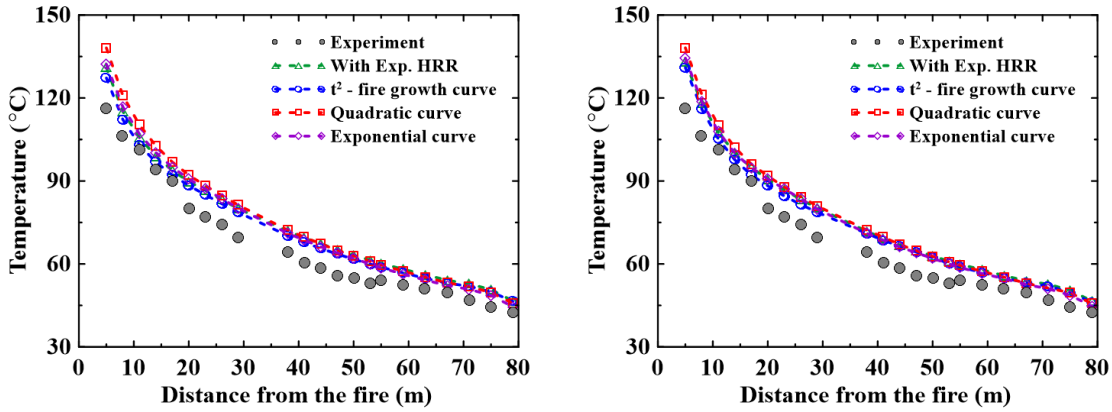

(a) MF (b) MCFC

Fig. 4. Longitudinal temperature distribution along the tunnel obtained by experiment and simulations with the experimental HRR and three DFCs.

and exponential DFCs. The fire growth rates of the quadratic and exponential DFCs were extremely low compared those of the experiment. In addition, the duration of the constant maximum HRR phase was negligible for the exponential DFC. Considering the fire growth rate and duration of the constant maximum HRR phase, the t^2-fire growth curve was the most reasonable among the DFCs in predicting fire development.

4.2 Temperature and smoke behavior

Temperature and smoke are important parameters that must be investigated in tunnel fire analysis to understand the possible fire spread behaviors and thermal damage to tunnel structures. The temperature depends on the fire development feature, which is directly related to the HRR of fire. Hence, in this study, the gas-phase temperature simulated with each DFC was investigated and compared with the experimentally measured smoke temperature.

Fig. 4 shows the longitudinal temperature distribution along the tunnel. The gas-phase temperatures predicted by the DFCs were compared with the experimental data. The average temperature from time interval 210 to 300 s was obtained when the HRR was in a quasi-steady state. The gas-phase temperature was measured at a height of 2.6 m from the floor. As shown in Fig. 4, the effects of the MF and MCFC models of the FDS in predicting the temperature were negligible. The temperatures predicted by the t^2-fire growth, quadratic, and exponential DFCs showed an exponential decay trend along the longitudinal direction, which was similar to the experimental temperature. The predicted results of each DFCs indicated reasonable agreement. In addition, the predictions of each of the DFCs did not differ significantly.

Smoke travel time (or smoke spread time) is a crucial parameter for understanding smoke spread and estimating the minimal time required for evacuation. In general, smoke spread can be identified by the substantial increase in temperature when high-temperature smoke flow reaches an assigned position, and the rate of smoke spread depends on the HRR of the fire. The temporal distributions of temperature and smoke at 150 s inside the tunnel are represented in Fig. 5. In the figure, the smoke distribution is represented by soot mass fraction. The high-temperature regions coincide well with those of high-concentration soot. The smoke spread predicted with the experimental HRR was faster than that predicted with the DFCs.

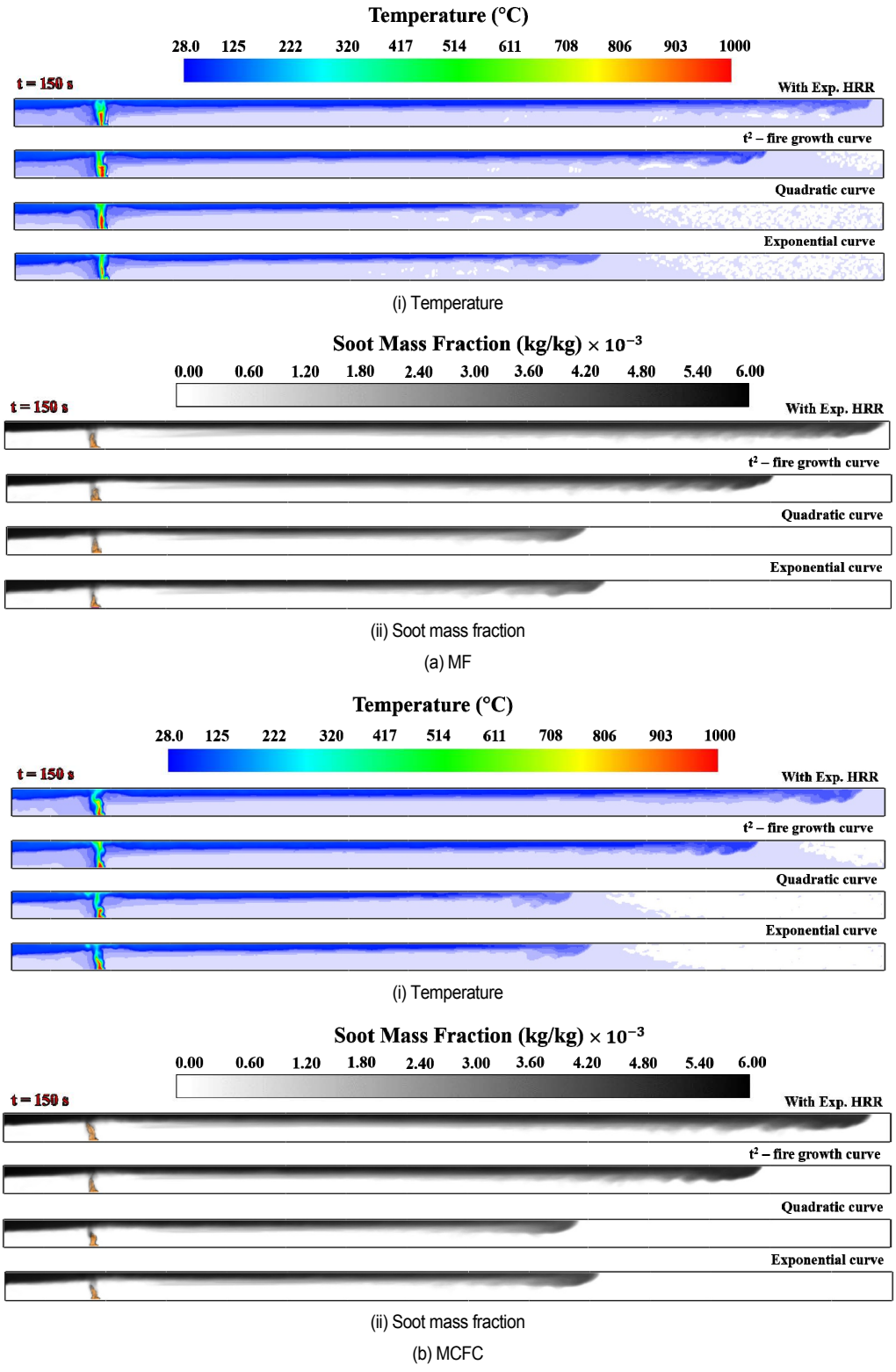

Fig. 5. Temperature and soot mass fraction inside the tunnel at 150 s.

The smoke travel time predicted by each input fire condition was in the following order, from the fastest to the slowest: experimental HRR > t^2-fire growth > exponential DFC > quadratic DFC. This was because the experimental HRR increased more rapidly than the other DFCs at the initial fire growth stage. The trend of smoke distribution at 150 s predicted by each input fire condition agreed well with that of the fire growth rate shown in Fig. 3. Similar to previous results for the HRR and temperature,

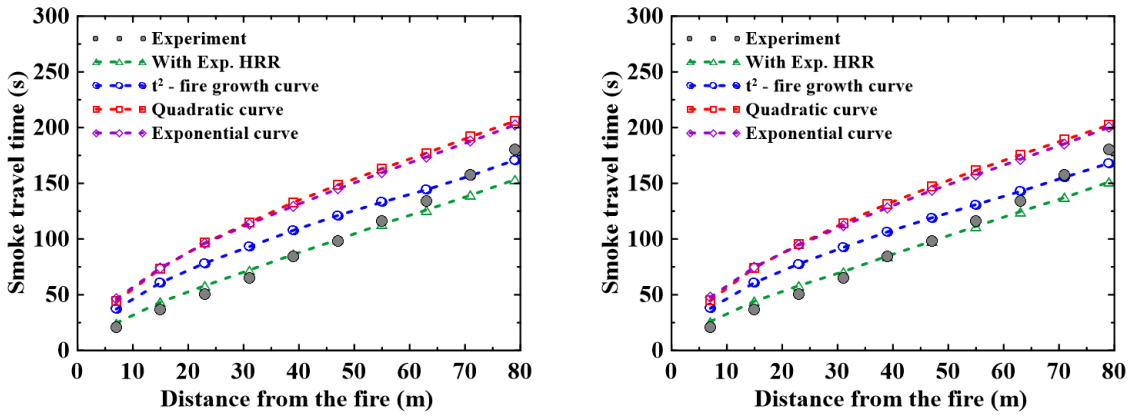

Fig. 6. Smoke travel time from the fire source obtained by experiment and simulations with the experimental HRR and three DFCs.

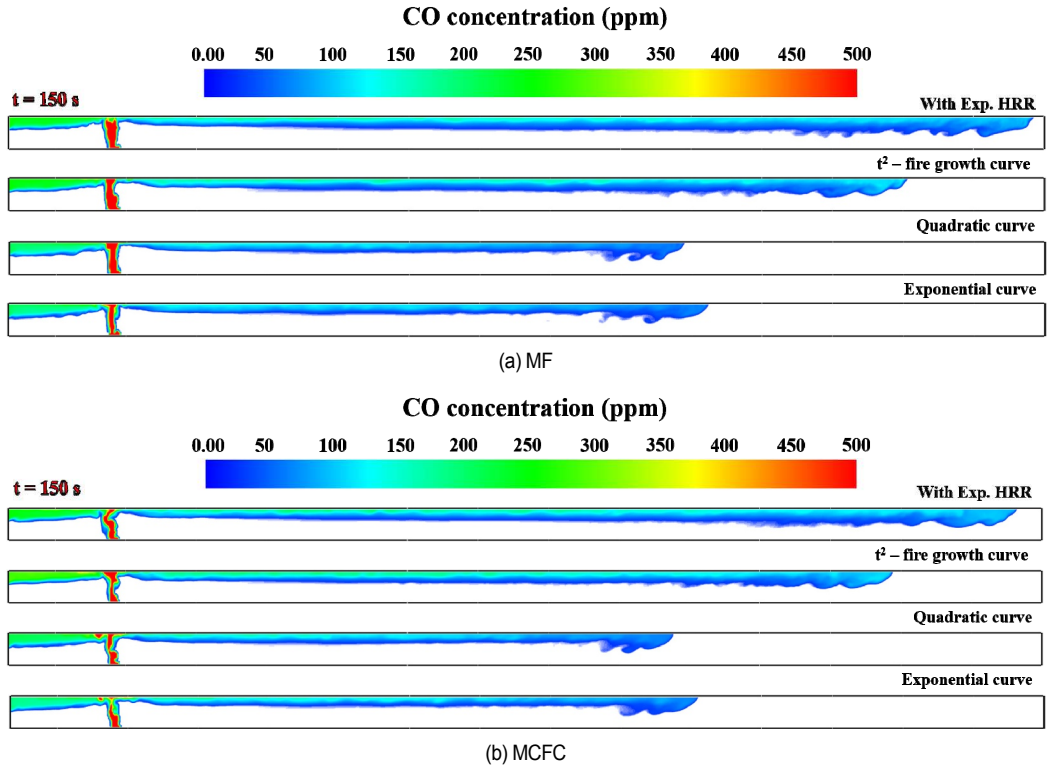

Fig. 7. CO concentration distribution inside the tunnel at 150 s.

the prediction performances of the MF and MCFC combustion models for smoke spread did not differ significantly.

Fig. 6 compares the longitudinal smoke travel time predicted by the experimental HRR and the t^2-fire growth, quadratic, and exponential DFCs. The smoke travel time was defined using the temperature difference in the tunnel, as in the experiment [7]. The overall comparison indicated that the smoke travel time predicted by experimental HRR agreed well with the experiment using both MF and MCFC models. The smoke travel time predicted by the t^2-fire growth curve was the most similar to that of the experiment. The smoke travel times predicted by the quadratic and exponential DFCs were almost similar but slower than that of the t^2-fire growth curve. These trends were almost identical to the smoke spread at 150 s. In other words, the initial fire growth rate of the input DFC significantly affected the smoke travel time in the tunnel.

4.3 CO behavior

CO is a crucial parameter for the analysis of toxic threats in fire risk assessments. CO is produced as a result of incomplete combustion and primarily occurs under under-ventilated fire conditions. Accurate predictions of CO production in fires are still actively investigated. Fig. 7 compares the CO spread inside

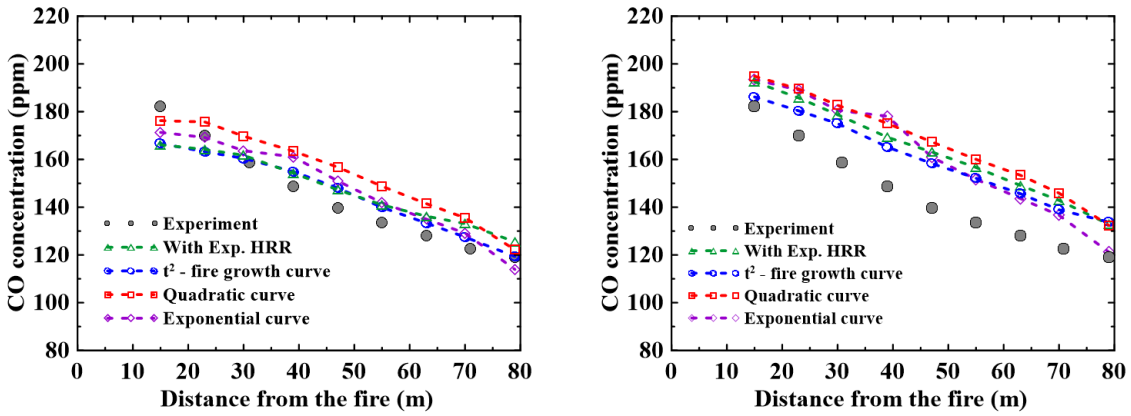

(a) MF (b) MCFC

Fig. 8. Longitudinal CO concentration along the tunnel obtained by experiment and simulations with the experimental HRR and three DFCs.

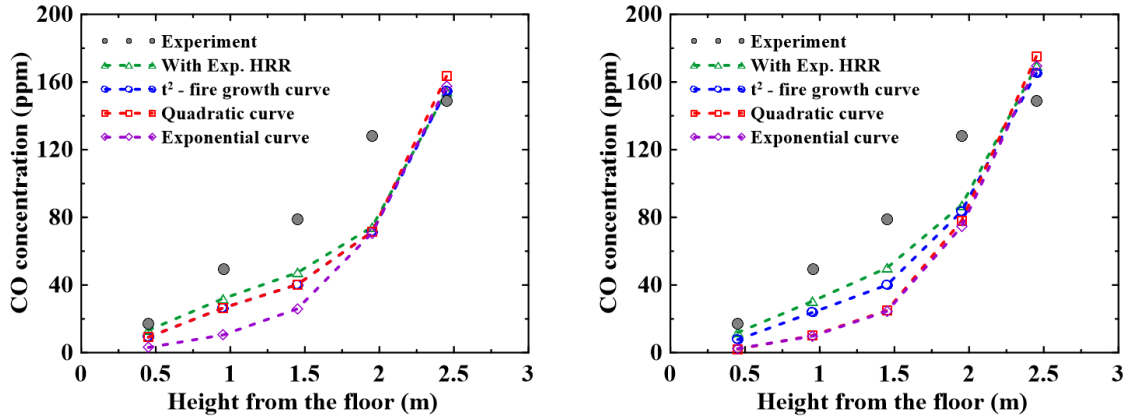

(a) MF (b) MCFC

Fig. 9. Vertical CO concentration at 39 m from the fire source obtained by experiment and simulations with the experimental HRR and three DFCs.

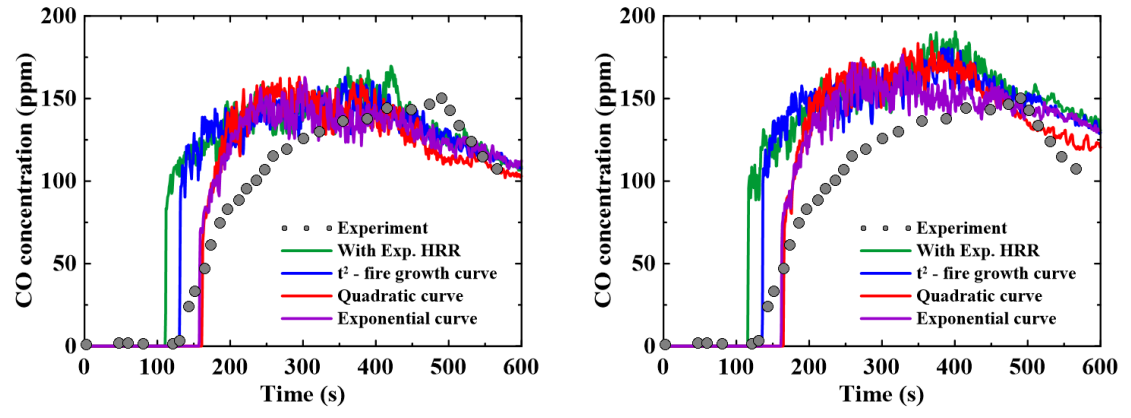

(a) MF (b) MCFC

Fig. 10. Temporal CO variation at 55 m from the fire source obtained by experiment and simulations with the experimental HRR and three DFCs.

the tunnel simulated with each DFC and two combustion models. CO spread is related to the smoke spread feature because the smoke carries the CO species. Hence, the trend of CO spread is the same as the trend of smoke spread, according to the DFCs shown in Fig. 5.

Fig. 8 shows the longitudinal CO concentration along the tunnel predicted by the t^2-fire growth, quadratic, and exponential DFCs. The CO concentration was measured at a height of 2.45 m and

averaged from 210 to 300 s when the HRR was in a quasi-steady state. The overall CO trend exhibited a gradual decrease with increasing longitudinal direction from the fire source.

The CO concentrations simulated with the MF model agreed reasonably well with the experimental results. The results predicted by the experimental HRR, t^2-fire growth, and exponential DFCs of the MF model indicated better prediction performances than those by the quadratic DFC for the experimental CO concentration. However, the MCFC model over-predicted the experimental CO concentration for all fire input conditions. In a previous numerical study of gas fire in a compartment, it was reported that the prediction performance of the MF model for CO concentration was better than that of the MCFC model [28]. Hence, the difference in the prediction performance of the two combustion models, MF and MCFC, was likely attributed to the same reasons as those reported by Baek et al. [28]. For the CO prediction of the MCFC model in the FDS, more detailed investigations are necessitated for various fire conditions.

Fig. 9 compares the vertical CO concentration predicted by each DFC with the MF and MCFC models. The vertical CO concentration was measured 39 m away from the fire source. The overall trend of the CO concentration in the experiment shows an approximately linear increase with the height above the floor. However, the simulation results show an exponential increase with the height. In particular, the simulation does not indicate reasonable agreement with the experiment at medium heights (1–2 m), whereas CO was well predicted by the simulation at the bottom (0.5 m) and upper heights (2.49 m). Considering both combustion models, the experimental HRR and t^2-fire growth curves demonstrated slightly better agreement for the experimental CO concentration than the other DFCs. This shows the limitation of the FDS for CO concentration in tunnel fires, similar to the description in Fig. 8.

Fig. 10 shows the variations in the temporal CO concentrations predicted by the DFCs based on the MF and MCFC models. The temporal CO concentration was measured 55 m from the fire source at a height of 2.2 m from the floor. The experimental CO concentration increased gradually from 125 to 500 s, followed by gradual decrease thereafter. However, the CO concentrations predicted by all input fire conditions, including the experimental HRR, exhibited a sharp increase initially. The increasing instants of each fire input condition were in the following order, from the fastest to the slowest: experimental HRR > t^2-fire growth > quadratic DFC ≈ exponential DFC, which was the same as the trend of DFCs in Fig. 3. The maximum CO concentration predicted by the MF model indicated better agreement with the experiment than the MCFC model, whereas both models did not predict the initial increase trend well. However, the t^2-fire growth curve predicted the instant of CO increase compared with the other DFCs. At this stage, the combination of the t^2-fire growth cure and MF combustion model yielded the best prediction performance among the DFCS. As mentioned previously, the initial fire growth rate of a DFC is important in the simulation of tunnel fires when a DFC is used as an input fire condition.

5. Conclusions

LES were performed using an FDS to investigate the prediction performance of t^2-fire growth, quadratic, and exponential DFCs for a tunnel fire experiment of 750 kW. For reference, an experimental HRR was adopted in the simulation as an input fire condition. The effects of FDS, MF, and MCFC combustion models were discussed.

The FDS yielded prediction performances that were similar to those of the MF and MCFC models, except for the CO concentration. For the latter, the two combustion models indicated some limitations in the simulations. However, the MF model demonstrated better prediction performances for the CO concentration and variation in time than the MCFC model.

The overall prediction performance of the input fire conditions in predicting the smoke behavior was in the following order, from the best to worst: experimental HRR > t^2-fire growth curve > quadratic DFC ≈ exponential DFC. A more accurate modeling of the fire growth rate for the initial fire stage was discovered to be important in the fire dynamics simulation of tunnel fires when a design fire curve was used in the simulation. In addition, the combination of a t^2-fire growth curve with an MF combustion model was the most effective combination for the fire simulation of tunnel fires. However, evaluation of DFC for various fire scenarios with different combustibles is required in the future work.

Acknowledgments

This research was carried out with the support from the field-based firefighting activity-supporting technology development project of the National Fire Agency (MPSS-Fire Safety-2015-66), Republic of Korea.

Nomenclature

Design fire curves

E_{tot}	: Total calorific value (kJ)
k	: Time width coefficient
n	: Retard index
$\dot{Q}$	: Heat release rate (kW)
$\dot{Q}_{max}$	: Maximum heat release rate (kW)
$\dot{Q}_{max,\ av}$	: Average maximum heat release rate (kW)
r	: Amplitude coefficient
t	: Time (s)
t_d	: Decay phase starting time (s) t^2-fire growth curve
t_D	: Decay phase starting time (s) quadratic curve
t_{end}	: End time of fire (s)
t_{lo}	: Level-off time (s)
t_o	: Ignition onset time (s)
α_d	: Fire decay rate (kW/s^2) t^2-fire growth curve
$\alpha_{D,q}$	: Fire decay rate (kW/s^2) quadratic curve
α_g	: Fire growth rate (kW/s^2) t^2-fire growth curve
$\alpha_{g,q}$	: Fire growth rate (kW/s^2) quadratic curve

Numerical methods

a, b, x, y, z : Mole proportions
C : Empirical constant
c_p : Specific Heat capacity (J/kg K)
$\frac{D}{Dt}$: Material derivative
D_α : Diffusion coefficient (m^2/s)
D_{LES} : Turbulent thermal diffusivity (kg /m s)
g : Gravitational acceleration (m/s^2)
h_s : Sensible enthalpy (kJ/kg)
h_α : Enthalpy of species α (kJ/kg)
k : Thermal conductivity (W /m K)
k_{LES} : Turbulent thermal conductivity (W /m K)
$k(T)$: Reaction rate constant (cm^3/mol s)
$\dot{m}_\alpha'''$: Volumetric mass production rate (kg/m^3 s)
$\dot{m}_{\alpha,1}'''$: $\dot{m}_\alpha'''$ in the first reaction step (kg/m^3 s)
$\dot{m}_{\alpha,2}'''$: $\dot{m}_\alpha'''$ in the second reaction step (kg/m^3 s)
p : Thermodynamic pressure (Pa)
Pr_t : Turbulent Prandtl number
$\dot{q}'''$: Heat release rate per unit volume (kW/m^3)
$\dot{q}'''_{max}$: Maximum $\dot{q}'''$ (kw/m^3)
$\dot{q}_r'''$: Net thermal radiation energy (kW/m^3)
$\dot{q}_r''$: Radiative heat flux (kW/m^2)
R : Universal gas constant (J/mol K)
s : Mass stoichiometric coefficient of oxygen
Sc_t : Turbulent Schmidt number
sgs : Sub-grid scale
t : Time (s)
T : Temperature (K)
u : Velocity vector (m/s)
W : Molecular weight of species (kg)
$x-(1-X_H)v_s$: Carbon atoms that not converted to soot.
X_H : Hydrogen fraction in soot
Y_α : Species mass fraction
y_{CO} : CO yield
Y_F^I : Mass fraction of fuel in the inlet stream
$Y_{N_2}^\infty$: Ambient mass fraction of nitrogen
$Y_{O_2}^\infty$: Ambient mass fraction of oxygen
y_s : Soot yield
Z : Mixture fraction (kg/kg)
Z_1, Z_2, Z_2 : Mixture fraction variables
α : General term to represent the gas species
ΔH_F : Heat of formation of fuel (kJ/mol)
ΔH_{CO} : Heat of formation of CO (kJ/mol)
$\Delta h_{f,a}^0$: Heat of formation of species α (kJ/mol)
ρ : Density (kg/m^3)
τ_{ij} : Viscous stress
τ_{ij}^{sgs} : Sub-grid scale (SGS) stress
τ_{ij}^{dev} : Total deviatoric stress
τ : Mixing time scale (s) MF model
τ_{mix} : Mixing time scale (s) MCFC model
μ : Dynamic viscosity (kg /m s)
v : Stoichiometric coefficient
δ : Kronecker delta
δx, δy, δz : Filter width size along x, y, and z directions (m)

References

[1] H. Ingason, Y. Z. Li and A. Lonnermark, *Tunnel Fire Dynamics,* Springer, New York (2014).
[2] Y. He, Smoke temperature and velocity decays along corridors, *Fire Safety Journal*, 33 (1) (1999) 71-74.
[3] Y. Wu and M. Z. A. Bakar, Control of smoke flow in tunnel fires using longitudinal ventilation systems – a study of the critical velocity, *Fire Safety Journal*, 35 (4) (2000) 363-390.
[4] L. H. Hu, R. Huo, Y. Z. Li, H. B. Wang and W. K. Chow, Full-scale burning tests on studying smoke temperature and velocity along a corridor, *Tunnelling and Underground Space Technology*, 20 (3) (2005) 223-229.
[5] L. H. Hu, R. Huo, W. Peng, W. K. Chow and R. X. Yang, On the maximum smoke temperature under the ceiling in tunnel fires, *Tunnelling and Underground Space Technology*, 21 (6) (2006) 650-655.
[6] L. H. Hu, R. Huo, H. B. Wang, Y. Z. Li and R. X. Yang, Experimental studies on fire-induced buoyant smoke temperature distribution along tunnel ceiling, *Building and Environment*, 42 (11) (2007a) 3905-3915.
[7] L. H. Hu, N. K. Fong, L. Z. Yang, W. K. Chow, Y. Z. Li and R. Huo, Modeling fire-induced smoke spread and carbon monoxide transportation in a long channel: Fire dynamics simulator comparisons with measured data, *Journal of Hazardous Materials*, 140 (1-2) (2007b) 293-298.
[8] L. H. Hu, J. W. Zhou, R. Huo, W. Peng and H. B. Wang, Confinement of fire-induced smoke and carbon monoxide transportation by air curtain in channels, *Journal of Hazardous Materials*, 156 (1-3) (2008) 327-334.
[9] L. H. Hu, F. Tang, D. Yang, S. Liu and R. Huo, Longitudinal distributions of CO concentration and difference with temperature field in a tunnel fire smoke flow, *International Journal of Heat and Mass Transfer*, 53 (13-14) (2010) 2844-2855.
[10] Y. F. Li, J. Bian and J. M. Li, Research on smoke flow in a tunnel fire of subway system, *Procedia Engineering*, 71 (2014) 390-396.
[11] A. Sojoudi, H. Afshin and B. Farhanieh, An analysis of carbone monoxide distribution in large tunnel fires, *Journal of Mechanical Science and Technology*, 28 (5) (2014) 1917-1925.
[12] H. Ingason, Design fire curves for tunnels, *Fire Safety Journal*, 44 (2) (2009) 259-265.
[13] L. Staffansson, *Selecting Design Fires*, Report 7032 Lund 2010, Department of Safety Engineering and Systems Safety, Lund University, Sweden (2010).
[14] H. J. Kim and D. G. Lilley, Heat release rates of burning items in fires, *38th AIAA Aerospace Sciences Meeting and Exhibit*, AIAA 2000-0722, Nevada (2000) 1-26.
[15] V. Babrauskas and R. D. Peacock, Heat release rate: The single most important variable in fire hazard, *Fire Safety Journal*, 18 (3) (1992) 255-272.
[16] H. Ingason, Fire development in large tunnel fires, *8th*

International Symposium on Fire Safety Science, Beijing (2005) 1497-1508.

[17] H. J. Kim and D. G. Lilley, Fire dynamic calculations and illustrations, *44th AIAA Aerospace Sciences Meeting and Exhibit, AIAA 2006-179*, Nevada (2006) 1-22.

[18] D. G. Lilley, Fire development calculations, *Journal of Propulsion and Power*, 16 (4) (2000) 641-648.

[19] B. Baek, C. B. Oh, E. J. Lee and D. G. Nam, Application study of design fire curves for liquid pool fires in a compartment, *Fire Science and Engineering*, 31 (4) (2017) 43-51.

[20] K. McGrattan, R. McDermott, S. Hostikka and J. Floyd, *Fire Dynamics Simulator (version 5.5) Technical Reference Guide*, National Institute of Standards and Technology, NIST Special Publication 1018-5 (2010a).

[21] K. McGrattan, R. McDermott, S. Hostikka and J. Floyd, *Fire Dynamics Simulator (version 5.5) User's Guide*, National Institute of Standards and Technology, NIST Special Publication 1019-5 (2010b).

[22] K. McGrattan, R. McDermott, S. Hostikka, J. Floyd, C. Weinschenk and K. Overholt, *Fire Dynamics Simulator (version 6.3.2) Technical Reference Guide*, National Institute of Standards and Technology, NIST Special Publication, 1018-1 (2015a).

[23] K. McGrattan, R. McDermott, S. Hostikka, J. Floyd, C. Weinschenk and K. Overholt, *Fire Dynamics Simulator (version 6.3.2) User's Guide*, National Institute of Standards and Technology, NIST Special Publication, 1019 (2015b).

[24] J. E. Floyd and K. B. McGrattan, Extending the mixture fraction concept to address under-ventilated fires, *Fire Safety Journal*, 44 (3) (2009) 291-300.

[25] D. Yang, L. H. Hu, Y. Q. Jiang, R. Huo, S. Zhu and X. Y. Zhao, Comparison of FDS predictions by different combustion models with measured data for enclosure fires, *Fire Safety Journal*, 45 (5) (2010) 298-313.

[26] G. H. Yeoh and K. K. Yuen, *Computational Fluid Dynamics in Fire Engineering Theory, Modelling and Practice*, Elsevier, Oxford (2009).

[27] Ü. Ö. Köylü and G. M. Faeth, Carbon monoxide and soot emissions from liquid-fueled buoyant turbulent diffusion flames, *Combustion and Flame*, 87 (1) 61-76.

[28] B. Baek, C. B. Oh, C. H. Hwang and H. S. Yun, Evaluation of the prediction performance of FDS combustion models for the CO concentration of gas fires in a compartment, *Fire Science and Engineering*, 32 (1) (2018) 7-15.

Dinesh Myilsamy is a Ph.D. student in the Department of Safety Engineering at Pukyong National University. He received his Master's degree in Safety Engineering in the year of 2017. His research interest include computational fire dynamics, and combustion engineering.

Chang Bo Oh is a Professor in the Department of Safety Engineering at Pukyong National University. He received his Ph.D. degree in Mechanical Engineering from Inha University, Korea, in 2003. His research interests include computations of safety-related problems, such as toxic chemical spread, combustion, fire and explosion.

Chi Young Lee is an Associate Professor in the Department of Fire Protection Engineering at Pukyong National University. He received his Ph.D. degree in Mechanical Engineering from KAIST, Korea. His research interests include fire and thermal-fluids engineering.